Title

Aberrant Development Corrected in Adult-Onset Huntington's Disease iPSC-Derived Neuronal Cultures via WNT Signaling Modulation.

Journal

Stem cell reports, 14(3)

ISSN

2213-6711

Authors

Smith-Geater, Charlene
Hernandez, Sarah J
Lim, Ryan G
et al.

Publication Date

2020-03-01

DOI

10.1016/j.stemcr.2020.01.015

Peer reviewed

Stem Cell Reports
Article

ISSCR

OPEN ACCESS

Aberrant Development Corrected in Adult-Onset Huntington's Disease iPSC-Derived Neuronal Cultures via WNT Signaling Modulation

Charlene Smith-Geater,[1,9] Sarah J. Hernandez,[2,9] Ryan G. Lim,[3] Miriam Adam,[4] Jie Wu,[5] Jennifer T. Stocksdale,[2] Brook T. Wassie,[6] Maxwell Philip Gold,[4] Keona Q. Wang,[2] Ricardo Miramontes,[3] Lexi Kopan,[2] Iliana Orellana,[3] Shona Joy,[7] Paul J. Kemp,[8] Nicholas D. Allen,[8] Ernest Fraenkel,[4,10] and Leslie M. Thompson[1,2,3,4,5,10,*]

[1]Department of Psychiatry and Human Behavior, University of California Irvine, Irvine, CA 92697, USA
[2]Department of Neurobiology and Behavior, University of California Irvine, Irvine, CA 96267, USA
[3]Department of Memory Impairment and Neurological Disorders, University of California Irvine, Irvine, CA 92697, USA
[4]Department of Biological Engineering, Massachusetts Institute of Technology, Cambridge, MA 02142, USA
[5]Department of Biological Chemistry, University of California Irvine, Irvine, CA 92617, USA
[6]LeadCrunch, San Diego, CA 92101, USA
[7]Neural Stem Cell Institute, Rensselaer, NY 12144, USA
[8]School of Biosciences, Cardiff University, Cardiff CF10 3AX, UK
[9]Co-first author
[10]Co-senior author
*Correspondence: lmthomps@uci.edu
https://doi.org/10.1016/j.stemcr.2020.01.015

SUMMARY

Aberrant neuronal development and the persistence of mitotic cellular populations have been implicated in a multitude of neurological disorders, including Huntington's disease (HD). However, the mechanism underlying this potential pathology remains unclear. We used a modified protocol to differentiate induced pluripotent stem cells (iPSCs) from HD patients and unaffected controls into neuronal cultures enriched for medium spiny neurons, the cell type most affected in HD. We performed single-cell and bulk transcriptomic and epigenomic analyses and demonstrated that a persistent cyclin $D1^+$ neural stem cell (NSC) population is observed selectively in adult-onset HD iPSCs during differentiation. Treatment with a WNT inhibitor abrogates this NSC population while preserving neurons. Taken together, our findings identify a mechanism that may promote aberrant neurodevelopment and adult neurogenesis in adult-onset HD striatal neurons with the potential for therapeutic compensation.

INTRODUCTION

Huntington's disease (HD) is an autosomal dominant CAG-repeat neurodegenerative disease (Huntington's Disease Collaborative Research Group, 1993). Mutation of the huntingtin (*HTT*) gene results in an expanded polyglutamine (Q^n) repeat within the HTT (mHTT) protein. Individuals with $\geq$40Q develop HD, with juvenile-onset cases before age 20 years typically occurring above 60 repeats (Cronin et al., 2019). HD symptoms include uncontrollable movement, psychiatric disturbances, and cognitive impairment (Tabrizi et al., 2019) with progressive neurodegeneration and brain atrophy. The primary cell type that degenerates is medium spiny neurons (MSNs) of the striatum, and there remain gaps in our knowledge of early and initiating events in HD systems.

Due to the degenerative nature of HD, postmortem human tissues limit our understanding of early neuropathology of affected brain regions. Human induced pluripotent stem cells (iPSCs) have emerged as important models to study neurodegenerative disease mechanisms (Poon et al., 2017). HD iPSCs differentiated to neural lineages have elucidated deficits in axonal guidance, lipid metabolism, and neuronal development and function (Conforti et al., 2018; HD iPSC Consortium, 2017; The HD iPSC Consortium, 2012), and dysregulation of the transforming growth factor β (Bowles et al., 2017; Ring et al., 2015), wingless-related integration site (WNT) (Lim et al., 2017), and p53 (Guo et al., 2013; Ring et al., 2015) signaling pathways.

Increased cell proliferation in HD patient brains proportional to disease grade in the subependymal layer that overlies the degenerating caudate nucleus (Curtis et al., 2003, 2005) suggests increased neurogenesis in the adult brain, potentially as an adaptation to disease. Using HD iPSC-derived neuronal cultures and differentiated embryonic stem cells (ESCs), dysregulation of neurodevelopmental pathways implicates deficits in striatal maturation (Wiatr et al., 2018). These signaling deficits occur early and are associated with phenotypes such as increased vulnerability to growth factor withdrawal in persistent neural progenitors (Mattis et al., 2014; Ring et al., 2015), suggesting that while neurogenesis is initiated, neuronal maturation may be impaired, leaving developmentally arrested cells vulnerable to cellular stressors. The mechanisms involved remain undefined, and these studies have primarily centered on highly expanded juvenile-onset repeat lines, with little known about the more prevalent adult-onset repeat-induced mechanisms.

Here, we use a multi-omics approach to investigate mHTT-associated molecular phenotypes using a modified protocol to differentiate HD patient iPSCs into highly pure populations of neurons with striatal characteristics. RNA sequencing (RNA-seq) and chromatin immunoprecipitation sequencing (ChIP-seq) analysis reveal significant dysregulation in cell-cycle-associated gene ontology (GO) terms. We show the persistence of a cyclin $D1^+$ mitotic cellular population that emerges among neural progenitors in adult-onset lines and is maintained through terminal differentiation. Single-cell RNA-seq (scRNA-seq) confirms that cell-cycle-related signaling cues arise from the mitotic population of cells, identified as neural stem cells (NSCs), rather than the striatal neurons present in the same population. Furthermore, we show that the persistence of NSC populations is the result of aberrant WNT signaling and we can ameliorate this population through WNT inhibition. This perhaps identifies a pathway or mechanistic target for future therapeutic exploration.

RESULTS

Modified Protocol for Differentiation of iPSCs to Pure Neurons for Epigenomic Study

Our goal was to define epigenetic signatures of neuronal cultures enriched for MSNs. iPSCs were differentiated to electrophysiologically active neurons (Arber et al., 2015; Telezhkin et al., 2016) with the addition of activin A to promote the formation of lateral ganglionic eminence (LGE)-like progenitors and the subsequent systematic programming of neural progenitors. Comparing the previous protocol (referred to as LI, due to the media containing LDN193189 and IWR1) (Telezhkin et al., 2016) to this protocol with addition of activin A (LIA = medium containing LDN193189, IWR1, and activin A), we observe an increase in the co-staining of Protein Phosphatase 1 Regulatory Inhibitor Subunit 1B (PPP1R1B, alias DARPP-32) and B-cell lymphoma/leukemia 11B (BCL-11B or CTIP-2) when tested on 33Q control neuronal cultures without any noticeable change to overall neuronal maturation, as seen using phase-contrast microscopy. There is no change in the proliferation of these cell lines at the neural progenitor day 16 stage (Figure S1). Four control lines (CS25iCTR18n2—18Qn2, CS25iCTR18Qn6—18n6, CS14iCTR28n6—28Qn6 [28Q], CS83iCTR33n1—33Qn1 [33Q]), two adult-onset lines (CS04iHD46n10—46Qn10 [46Q] and CS03iHD53n3—53Qn3 [53Q]), and three juvenile-range repeat lines (CS02iHD66n4—66n4 [66Q], CS81iHD71n3—71n3 [71Q], CS09iHD109n1—109n1 [109Q]) were differentiated over 37 days to mature neuronal cultures in duplicate (18Qn2, 46Q) or triplicate (18Qn6, 28Q, 33Q, 53Q, 66Q, 71Q, 109Q) (Figure 1). Quality control measures were performed (Table S1). To control for sex effects, these lines include male (18Q, 46Q, 53Q) and female subjects (28Q, 33Q, 66Q, 71Q, 109Q). Mature neurons were defined by microtubule-associated protein 2 (MAP-2) expression and striatal neurons by DARPP-32 and BCL-11B co-staining (Figure S2); quantification can be found in Table S1. The 46Q iPSC line was the only sample not to reach 10% DARPP-32 expression in the total population following differentiation (Table S1). As this differentiation protocol provides a high percentage of mature neurons (79%–98% $MAP\text{-}2^+$ for all cell lines), the following data represent a multi-omics analysis of mature neuronal cultures enriched for striatal characteristics derived from iPSCs within the context of HD.

Transcriptomics Reveal an Upregulation of Cell-Cycle-Related Genes in HD

Bulk, total RNA-seq was used to identify differentially expressed genes (DEGs) between control and HD mature neuronal cultures enriched for MSNs. Gene expression values and DEGs were used for principal component analysis (PCA), GO enrichment analysis (GOrilla) and Ingenuity Pathway Analysis. Curiously, PCA of control (red) and juvenile-repeat range (green) lines shows no clear separation (Figure S3). Only 105 DEGs were identified (Table S2, columns A–H) when comparing highly expanded repeat lines with controls, and there was no enrichment for specific GO terms, although RE1 Silencing Transcription Factor (REST) was downregulated as described in neural cultures (Buckley et al., 2010; HD iPSC Consortium, 2017). Finding limited DEGs was surprising given the documented transcriptional dysregulation in HD and in models expressing juvenile-range repeat lengths (Valor, 2015). Control (red) and adult-onset (blue) lines, however, show separation along principal component 1 (PC1) (Figure 2A). Given the statistical difference between the control and adult-onset lines and the biological relevance of exploring CAG-repeat lengths more prevalent in the HD population, we continued our analysis to define transcriptional differences between control and adult-onset lines. We identified 823 DEGs in adult-onset neuronal cultures enriched for MSNs compared with control lines (10% false discovery rate [FDR] cutoff), with 754 genes upregulated and 69 genes downregulated (Table S2, columns I–P). The top genes by adjusted p value are labeled in a volcano plot (Figure 2B). Interestingly, the second most statistically significantly upregulated gene was the pluripotency marker POU domain, class 5, transcription factor 1 (*POU5F1*, alias *Oct4*) whereas other markers of pluripotency were not dysregulated (NANOG homeobox gene [*NANOG*], Podocalyxin like [*PODXL*, alias *TRA-1-81*], Kruppel-like factor 4 [*KLF4*], MYC proto-oncogene [*MYC*]). GO enrichment revealed dysregulation of cell-cycle-associated biological processes

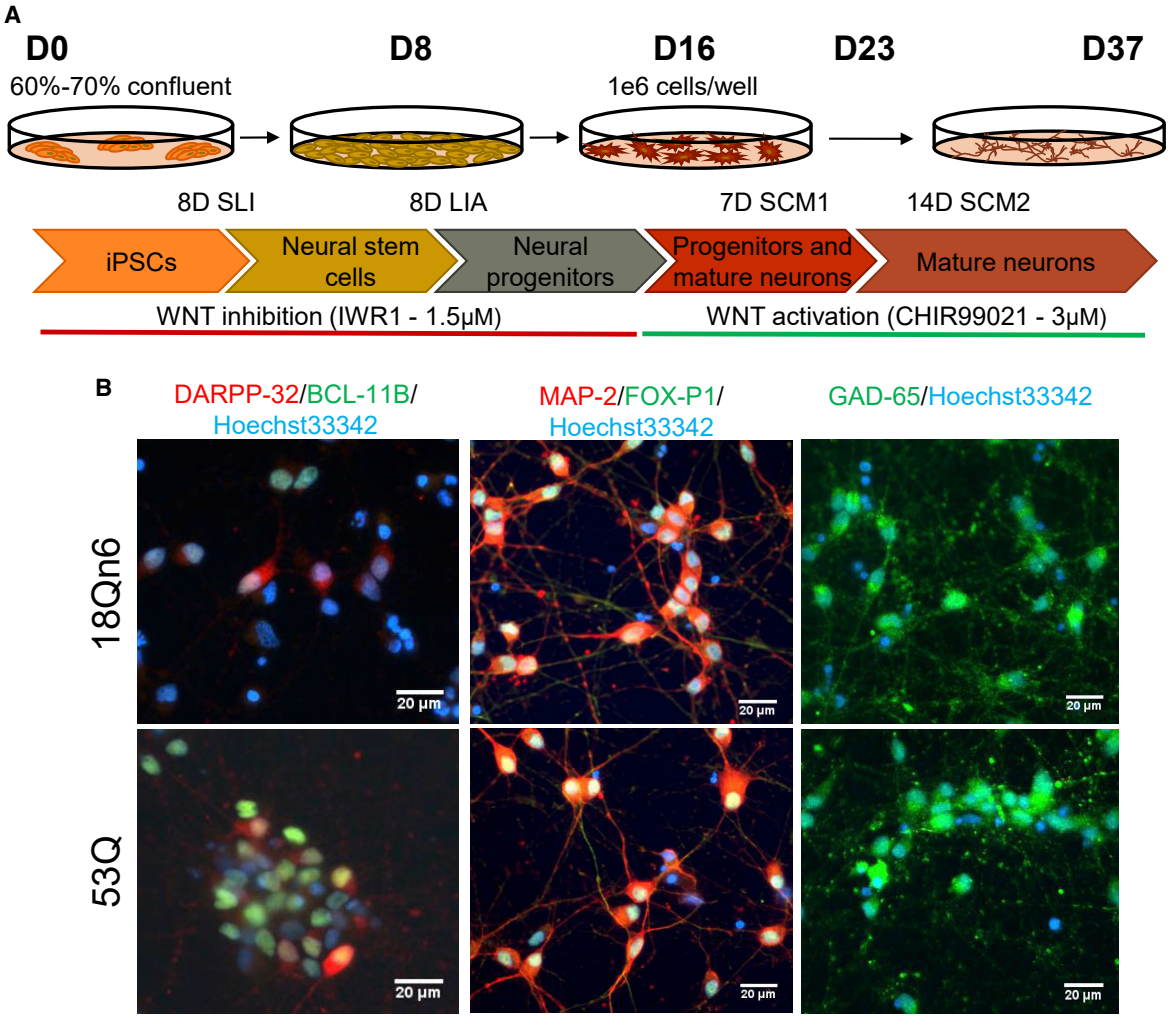

Figure 1. Differentiation Protocol for iPSC-Derived Striatal Neuronal Cultures

(A) Schematic of the differentiation protocol used for iPSC-derived striatal neurons enriched for medium spiny neurons (MSNs) adapted from Telezhkin et al. (2016).

(B) Representative immunofluorescence images of cells at day 37 in control (top) and HD (bottom) cells showing that the cells are positive and co-localize for DARPP-32 and BCL-11B (left); cells are also positive for FOX-P1 and MAP-2 (middle) and are GABAergic, as they express the glutamate decarboxylase-2 enzyme (right). Scale bar, 20 μm.

(Figure 2C), DNA-binding-associated molecular functions (Figure 2D), and chromosomal gene-associated cellular components (Figure 2E). The top cellular function, predicted to be activated, is cell-cycle progression, with a p value of 7.57×10^{-39}.

Upregulation of Cell-Cycle-Related Genes and Transcription Factors in HD Identified Using Epigenomic Analysis

We performed ChIP-seq on trimethylated, histone 3 lysine 4 (H3K4me3) residues to identify active promoters in control (18Qn2, 18Qn6, 28Q, 33Q) and HD (46Q, 53Q) neuronal cultures, whereby 99,765 K4me3 sites were found across the lines. Differential analysis of K4me3 occupancy between control and HD lines identified 2,153 sites (5% FDR cutoff); 1,133 of the sites had higher K4me3 levels in HD and 764 sites had higher levels in controls. PCA of differential peaks (Figure 3A) shows clear separation between control and HD K4me3-enriched signals. Differential peaks were annotated to 1,340 genes within a window of 10 kb from transcription start sites (TSS), with a majority of the genes (1,143 genes) having an upregulated K4me3 signal in HD. GO enrichment analysis of the genes annotated to the differential sites shows enrichment of cell-cycle-related terms (Figure 3B).

We overlapped the ChIP-seq and RNA-seq differential signals and found that almost half of the transcriptionally

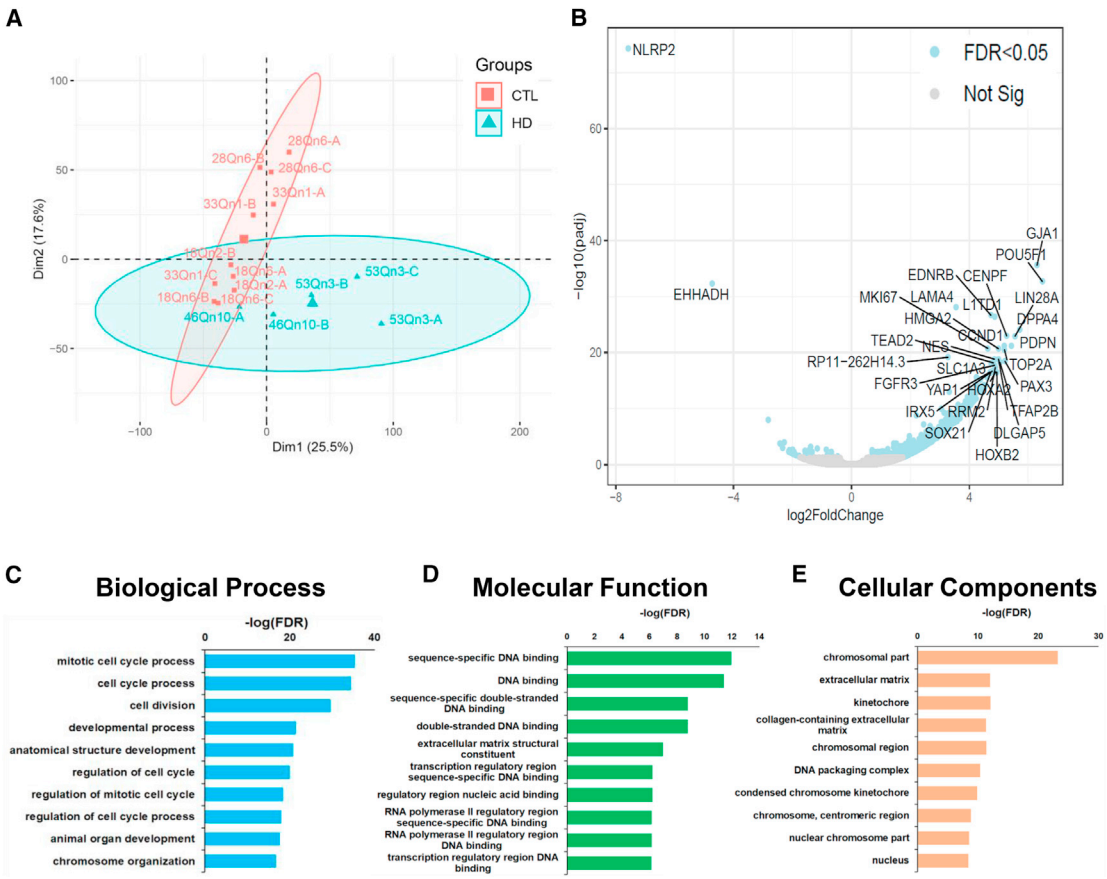

Figure 2. Cell-Cycle-Related Genes Are Upregulated in HD Adult-Onset Cell Lines by RNA-Seq

(A) PCA of global gene expression in HD (46Q and 53Q) and control (18Q, 28Q, and 33Q) iPSC-derived striatal neurons. PC1, which captures the most gene expression variance between samples, shows separation of HD and control samples.

(B) Volcano plot showing statistically significant DEGs (light blue) between HD (46Q and 53Q) and control (18Q, 28Q, and 33Q) samples. The most significant genes, by FDR, are labeled. Significant gene expression differences are skewed, showing many more upregulated DEGs in the HD samples (Table S2, columns A–H).

(C–E) Top GO enrichment analysis terms for biological process (C), molecular function (D), and cellular components (E) showing enrichment for cell cycle, DNA binding, extracellular matrix, and chromosomal genes.

upregulated genes in HD (327 DEGs) had K4me3-upregulated sites in the area next to their TSS (Figure 3C). The subset of genes upregulated both transcriptionally and epigenetically show higher enrichment for cell-cycle GO terms (compare Figures 3D and 3B). We used Assay for Transposase-Accessible Chromatin sequencing (ATAC-seq) data to localize the transcription factor (TF)-binding sites within the K4me3 differential sites adjusted to the upregulated DEGs. TF analysis of these sites suggests enrichment for binding of several TFs related to cell-cycle regulation in HD lines (Figure 3E).

Adult-Onset HD Cell Lines Have a Persistent Mitotically Active Population in Neuronal Cultures

Additional adult-onset HD lines were added to the study to determine whether the altered mitotic signature was maintained across different subjects. Within each of the terminally differentiated adult-onset lines, we observe novel populations comprising cells with enlarged cell bodies that lack projections, which are quite distinct from neurons and are absent in control cell lines (Figure 4A). These morphologically distinct cell clusters are readily apparent at the end of culture, as identified by phase-contrast microscopy. These cells are visible at low frequency at day 18 and are observed at higher frequency by day 23 among differentiating neurons. These cell clusters are present in each of four adult-onset HD cell lines examined (CS13iHD43n13 [43Q], 46Q, CS87iHD50n7—50Qn7 [50Q], 53Q) by immunofluorescence and phase-contrast microscopy (Figures S4A and S4B). These aberrant cells are positive for the cell-cycle G_1/S phase transition marker cyclin D1, the pluripotency marker Oct4, and

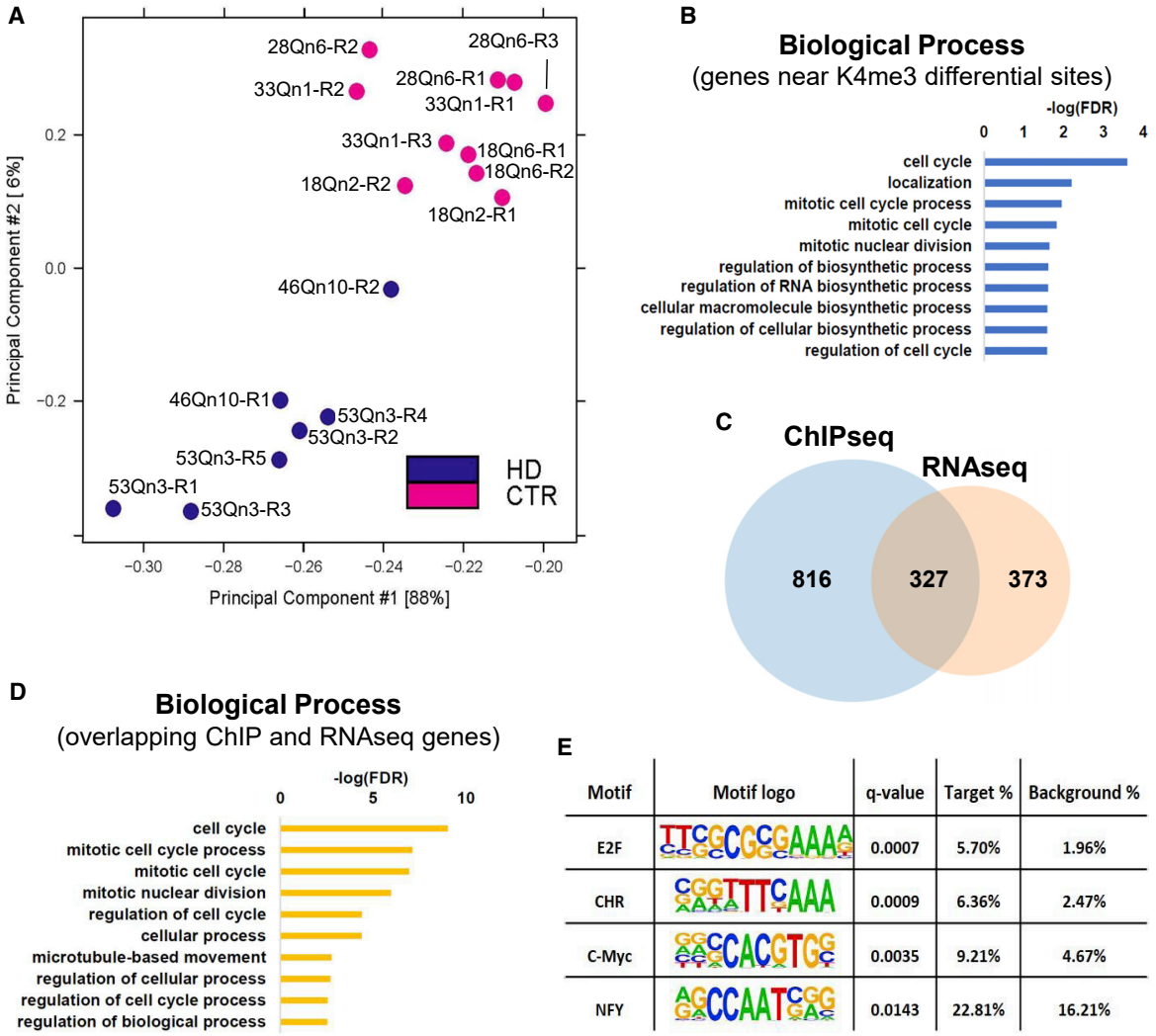

Figure 3. Epigenomics Upregulation of Cell-Cycle-Related Genes in HD

(A) PCA of K4me3 sites identified by ChIP-seq in HD (46Q and 53Q) and control (18Q, 28Q, and 33Q) iPSC-derived striatal neurons.

(B) Top GO enrichment analysis terms for genes near K4me3 differential sites show enrichment for cell cycle.

(C) Venn diagram of genes upregulated in HD in RNA-seq and ChIP-seq. Upregulated K4me3 sites were found near the TSS of almost half of the transcriptionally upregulated genes in HD.

(D) Top GO enrichment analysis terms for the RNA and ChIP-seq overlapping genes show enrichment for cell-cycle processes.

(E) Transcription factor (TF) analysis of the regulatory sites near genes upregulated in both RNA and ChIP-seq. Cell-cycle-related TF-binding sites are enriched in HD.

the neuroectoderm marker nestin, and are negative for the neuronal marker MAP-2 (Figure 4B), an unexpected finding given that the differentiation protocol produces terminally differentiated, post-mitotic, mature neurons. This population is not the result of the LIA-adapted neural progenitor specification adopted in our protocol, as it is also observed using the previously published LI protocol (Telezhkin et al., 2016) (Figures S1D and S4A), which is important given the role that activin A can play in pluripotency (Beattie et al., 2005).

Flow cytometry was used to quantify the percentage of the population composed of cyclin $D1^+$ cells, which revealed a significant increase ($p = 0.0003$) of cyclin $D1^+$ cells (48.46% ± 4.54%) in terminally differentiated HD lines compared with controls (3.654% ± 1.206%) when grouped together (Figure 4C). Separately, HD lines (50Q, 53Q) have significantly more cyclin $D1^+$ cells than controls (18Qn6 [18Q], CS71iCTR20n6—20Qn6 [20Q]) (Figure S4C). Almost all of the cyclin $D1^+$ cells were also nestin positive (98.5% ± 0.55%) and a high proportion of them were Oct4 positive

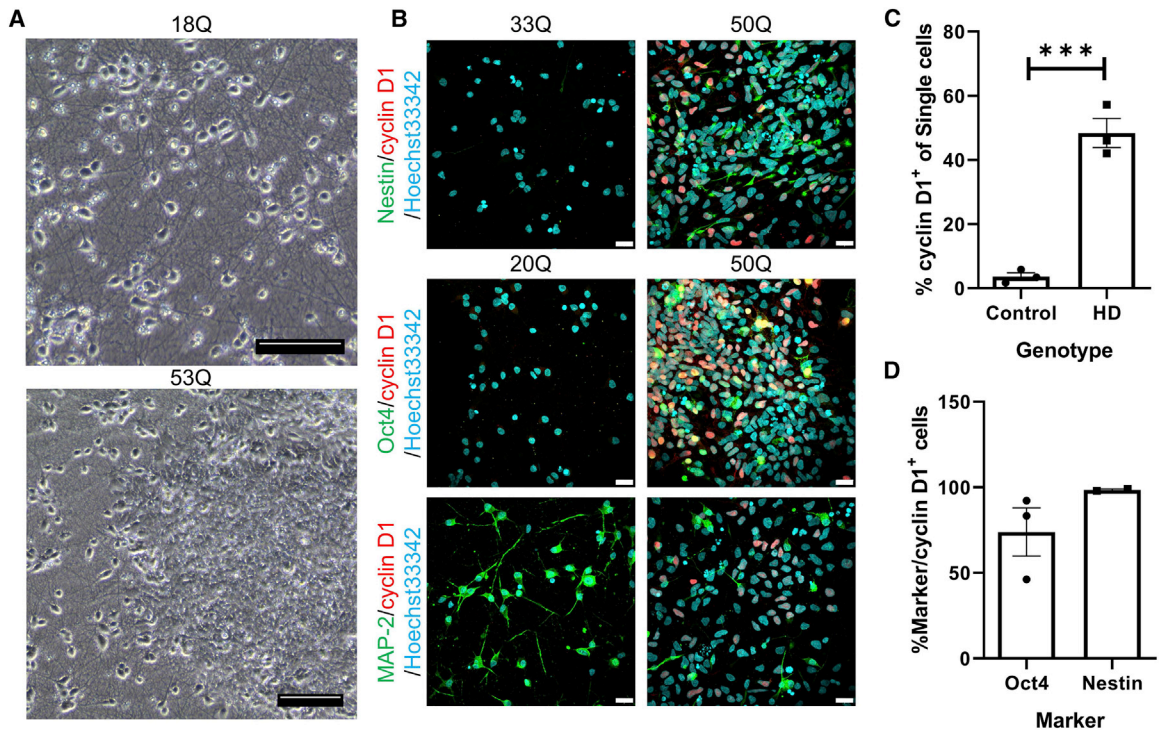

Figure 4. High Percentage of Adult-Onset HD Neuronal Populations Express Cyclin D1 Compared with Controls

(A) Phase-contrast images show control (top) and HD (bottom) neurons, with the mitotic population persisting in the HD line occupying the majority of the field. Scale bar, 100 μm.

(B) Assessment of the cyclin D1$^+$ population by immunofluorescence shows co-staining of cyclin D1 with nestin (top) and Oct4 (middle), and no co-staining with MAP-2 (bottom). Scale bar, 20 μm. Images are representative of the four adult-onset lines tested (43Q, 46Q, 50Q, 53Q), quantification for which can be found in Figure S4A.

(C) Analysis of cyclin D1 expression by flow cytometry shows a significant increase in percentage of cells expressing cyclin D1 compared with controls. Data were acquired across three experiments using three cell lines per condition for two experiments (18Q, 20Q, 33Q, 46Q, 50Q, 53Q) and one experiment with two lines per condition (18Q, 20Q, 50Q, 53Q). Data represent mean ± SEM. Unpaired one-tailed t test, t = 9.539, df = 4, p = 0.0003, ***p < 0.001.

(D) Analysis of co-markers of HD cyclin D1$^+$ cells by flow cytometry shows that the majority of cyclin D1$^+$ cells are Oct4$^+$ and nestin$^+$. Data from 50Q and 53Q (nestin), n = 1 HD cell line; data from 46Q, 50Q, 53Q (Oct4), n = 2 HD cell lines. Data represent mean ± SEM.

(73.9% ± 14.1%) (Figure 4D), implying that Oct4 and nestin are expressed in the same cells in a large proportion of the cyclin D1$^+$ population. Of the total day-37 population, Oct4 was expressed at very low levels in control cells (1.03% ± 0.20%) and higher in adult-onset HD cells (22.7% ± 4.34%) (Figure S5). Importantly, there was a very low percentage (<0.054%: 20Q, 46Q, 50Q) of Oct4-positive cells in cultures at early stages (day 8) (Figure S5). Cyclin D1$^+$ cells are proliferative throughout terminal differentiation, and increasingly make up more of the total population as the number of days *in vitro* progresses; however, this does not seem to have a detrimental effect on the remaining post-mitotic neurons.

Single-Cell RNA-Seq Identifies the Cyclin D1$^+$ Population Specific to Adult-Onset Lines as NSCs

To define the composition of the persistent cyclin D1$^+$ cell population present in HD cultures, we performed scRNA-seq on neuronal populations differentiated from one representative control (18Qn6—18Q) and HD iPSC line (53Q). Single-cell viability for each sample was determined (86.9% for 18Q, 80.9% for 53Q). The estimated number of cells sampled was 5,070 (18Q) and 3,829 (53Q) with an average number of reads per cell of 31,675 (18Q) and 41,939 (53Q). After quality control of data filtering, the data were aggregated using Cell Ranger and gene-by-cell expression matrices generated and used as input for Seurat and Scanpy. The top variable genes by PCA were used for exploratory analysis and visualization using t-distributed stochastic neighbor embedding (t-SNE) (Figure 5A). An unsupervised clustering approach identified seven distinct cell clusters, which were annotated using known cell-type markers (Figure 5B and data not shown). The NSC cluster (Figure 5A) is specific to the HD cell line, with the remaining clusters contributed to by both cell lines. None of the

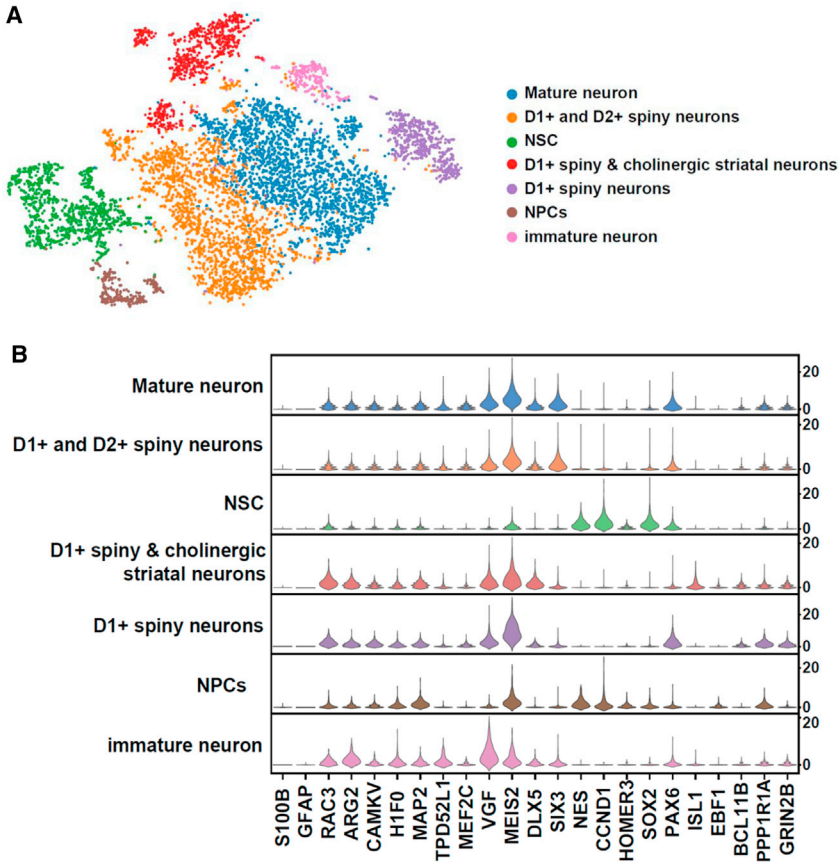

Figure 5. scRNA-Seq Reveals a Unique Population of Cells Only in the Adult HD Sample

(A) t-SNE plot of the aggregated scRNA-seq data from both the control (18Q) and HD (53Q) samples showing seven cell clusters. Clusters were annotated using known cell-type marker genes and are: mature neuron (blue; TPD52 like 1 [*TPD52L1*], myocyte enhancer factor 2C [*MEF2C*], paired box 6 [*PAX6*], and SIX homeobox 3 [*SIX3*]); D1 and $D2^+$ spiny neurons (orange; Meis homeobox 2 [*MEIS2*], distal-less homeobox 5 [*DLX5*], hippocalcin [*HPCA*]); NSC cluster (green; nestin [*NES*], cyclin D1 [*CCND1*]); $D1^+$ spiny and cholinergic striatal neurons (red; *DLX5*, ISL LIM homeobox 1 [*ISL1*], Rac family small GTPase 3 [*RAC3*], arginase 2 [*ARG2*]); $D1^+$ spiny neurons (purple; *MEIS2*, protein phosphatase 1 regulatory inhibitor subunit 1A [*PPP1R1A*], CaM kinase-like vesicle associated [*CAMKV*], *RAC3*, glutamate ionotropic receptor NMDA type subunit 2B [*GRIN2B*]); neural progenitor cells (NPCs) (brown; *CCND1*, homer scaffold protein 3 [*HOMER3*], EBF transcription factor 1 [*EBF1*]); and immature neurons (pink; VGF nerve growth factor inducible [*VGF*], H1 histone family member 0 [*H1F0*]). (B) Stacked violin plot showing expression of glial, neural, and neuronal cell-type markers. *CCND1* expression is mainly visible in the NSC cluster, which only exists in the HD (53Q) sample.

clusters express the astrocyte marker S100 calcium-binding protein β (*S100β*) or glial fibrillary acidic protein (*GFAP*), and most clusters express the neuronal marker *MAP2*, with the neural progenitor marker *NES* only expressed in the green and brown clusters. Only the NSC cluster in the HD line had high levels of *CCND1*. *CCND1* identifies the aberrant HD population, and we find that other genes are also upregulated in this cluster that are either lowly or not expressed in the other six clusters (Table S2, columns Q–V), including the progenitor marker *NES* and SRY-box transcription factor 2 (*SOX2*), which identifies these cells as an NSC-type population.

While the signal from the NSCs likely obscured gene expression differences from the neuronal population in our bulk RNA-seq dataset, scRNA-seq allowed for the identification of gene expression differences in $MAP2^+$, $NES/SOX2^-$ neurons between HD and control lines (Table S2, columns W–AB). In this population, genes known to be dysregulated in HD were observed, some of which are: activity-regulated cytoskeleton associated protein (*ARC*), Fos proto-oncogene, AP-1 transcription factor subunit (*FOS*), JunB proto-oncogene, AP-1 transcription factor subunit (*JUNB*), neuronal PAS domain protein 4 (*NPAS4*), and neurogranin (*NRGN*), suggesting the possibility that these populations contribute to previously defined HD molecular signatures.

Inhibition of the WNT Signaling Pathway Abrogates NSC Populations in HD Neuronal Cultures

Two of the top three transcriptional regulators with the largest changes in RNA-seq expression are transcriptionally regulated by WNT signaling: *Oct4* (*POU5f1*, 6.479-fold increase) and *CCND1* (5.186-fold increase). Analysis of TF-binding sites demonstrates that two of the top four regulatory motifs near genes upregulated in both RNA-seq and ChIP-seq are *MYC* and *E2F*, which are both involved with WNT signaling (Hughes and Brady, 2005; Shi et al., 2015; Yeo et al., 2011) (Figure 3E). Examination of the WNT/β-catenin signaling pathway reveals significant dysregulation of several key members, including components of the β-catenin destruction complex, APC regulator of WNT signaling pathway (*APC*), and glycogen synthase kinase 3β (*GSK3β*) downregulated in HD lines (Figure 6A). Additionally, scRNA-seq demonstrates that

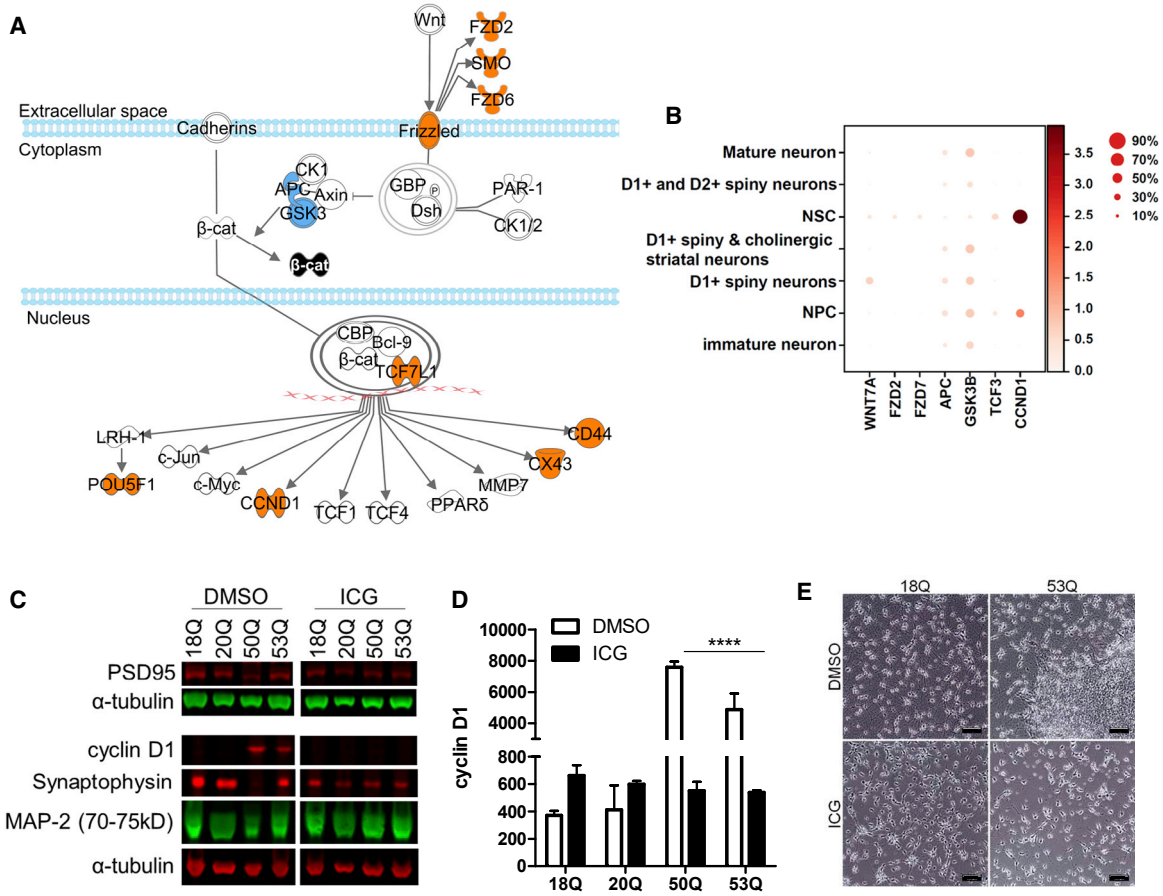

Figure 6. WNT/β-Catenin Signaling Is Significantly Dysregulated and WNT Inhibition Rescues Aberrant Cyclin D1 Overexpression while Abrogating the Mitotic Population of Cells in Adult-Onset Neurons

(A) Dysregulation of the WNT/β-catenin signaling pathway from bulk RNA-seq was analyzed using Ingenuity Pathway Analysis. While Frizzled receptors are upregulated, members of the β-catenin destruction complex, specifically *APC* and *GSK3β*, are downregulated, allowing for upregulation of WNT/β-catenin transcriptional targets, such as *CCND1* and Oct4 (*POU5F1*). Orange molecules are upregulated, blue are downregulated, and black are targeted for destruction. A full legend can be found in Figure S5. 46Q and 53Q lines were compared with controls with 18Q (2 clones), 28Q, and 33Q in triplicate using a 0.1 FDR.

(B) Dot plots show expression of WNT/β-catenin pathway genes and *CCND1*. The NSC cluster shows higher expression of all WNT-related genes except for genes of the destruction complex, *APC* and *GSK3β*, and *WNT7A*, which shows higher expression in the NSC cluster over all other clusters besides the cortical cluster.

(C) The WNT inhibitor ICG or DMSO was added to the NPC population at day 16 of differentiation. Cells were harvested at day 37 and western blots were performed for cyclin D1, MAP-2, synaptophysin, and PSD95 using LI-COR.

(D) Quantitation demonstrates that treatment with ICG completely rescues aberrant overexpression of cyclin D1 in adult-onset striatal neurons (50Q and 53Q). For analysis, lines were grouped by genotype. White bars represent DMSO-treated cells and black bars represent ICG-treated cells. Analysis was done using a two-way ANOVA with Bonferroni correction. Multiplicity-adjusted p values were calculated for each comparison at a 95% confidence interval. Data represent mean ± SEM. ****$p < 0.0001$. Data are from two independent experiments using four cell lines grouped by control (18Q, 20Q) and HD (50Q, 53Q). Further statistical details can be found in Tables S3 and S4.

(E) Representative phase images show the mitotic population of cells at day 37 in adult-onset line (53Q) treated with DMSO (top-right panel), which is completely abrogated by ICG addition (bottom-right panel). The 53Q line is a representative adult-onset line. Scale bar, 100 μm.

the dysregulation we observe in the WNT/β-catenin signaling pathway from the bulk analysis resides in the NSC population, which has increased expression of Wingless-Type MMTV Integration Site Family, Member 7A (*WNT7A*), increased expression of Transcription Factor 3 (TCF3), increased expression of frizzled transcripts (frizzled class receptor 2 [*FZD2*] and frizzled class receptor 7 [*FZD7*]), decreased expression of β-catenin destruction complex

transcripts (*APC* and *GSK3β*), and increased expression of WNT transcriptional targets (*CCND1*) (Figure 6B). We were unable to detect *POU5f1* expression in many of the HD cells (about 90 positive cells in HD lines and three positive cells in controls), presumably due to lower sequencing depth using the scRNA-seq platform.

Because of the regulatory role of WNT/β-catenin over the expression of mitotic and pluripotency genes, we hypothesized that downstream correction of the WNT/β-catenin signaling pathway might reduce the mitotic cues necessary for the persistence of the NSC population in HD lines. Therefore, we titrated several WNT inhibitors that act downstream of the β-catenin destruction complex and found that the addition of ICG-001 (hereafter ICG) eliminates the mitotic cell population within HD neuronal cultures. ICG is a selective, potent inhibitor of β-catenin-mediated transcription by preventing the interaction between CREB-binding protein and β-catenin (Emami et al., 2004). ICG addition at day 16 in the differentiation protocol significantly reduced cyclin D1 protein expression in HD lines (50Q, 53Q) by a factor of 10 (Figures 6C and 6D). A highly expanded repeat line (109Q) was assessed to determine the potential effect of ICG based on polyQ length; however, no additional effect was observed (Figure S6). Representative phase-contrast images of a representative adult-onset line (53Q; Figure 6E) demonstrate that ICG treatment abrogates the morphologically distinct NSC populations within adult-onset HD neuronal cultures. Additionally, ICG does not alter MAP-2 expression (Figure S6A), suggesting that the presence of neurons is not altered by treatment. While expression of synaptophysin and Disks Large MAGUK Scaffold Protein 4 (alias PSD95) remain unchanged in HD lines (Figures S6B and S6C), expression of both is reduced in control lines by ICG treatment (Figure S6B). Notably, for these differentiations the 50Q line overwhelmingly had the highest percentage of mitotic cells and therefore, correspondingly, DMSO-treated 50Q cells have the lowest levels of MAP-2, PSD95, and synaptophysin overall.

DISCUSSION

Multi-omics-level analyses were performed on HD neuronal cultures enriched for MSNs using a protocol that induces increased expression of LGE markers including distal-less homeobox 1 and 2 (*DLX1/2*) and GS homeobox 2 (*GSX2*) mRNA. This response is likely via upregulation of BCL-11B, which is important for MSN development (Arlotta et al., 2008). Introduction of activin A increased co-localization of BCL-11B and DARPP-32$^+$ neurons, which is more indicative of MSNs than DARPP-32 positivity alone (Carri et al., 2013). Total RNA-seq and scRNA-seq showed that the primary transcriptional differences were reflected in a persistent population of NSCs within terminally differentiated, post-mitotic neuronal cultures from patients with adult-onset repeats. These findings are consistent with mitotic aberrations found in HD iPSCs differentiated toward a striatal lineage (Mattis et al., 2014). Here, we uncover a key mechanism underlying this mitotic persistence.

mHTT has an impact on neurogenesis in HD knockin (Molero et al., 2009), transgenic R6/1 (Lazic et al., 2004), and R6/2 (Phillips et al., 2005) mouse models, and patient postmortem tissue (Curtis et al., 2003, 2005). Neurodevelopmental changes associated with mHTT expression are observed in other stem cell-derived models: *HTT*-null NSCs derived from mouse ESCs (Lo Sardo et al., 2012), HD patient-derived iPSC striatal cells (Conforti et al., 2018), and an isogenic allelic series of human ESCs differentiated toward a cortical neuron fate form disorganized neural rosettes (Ruzo et al., 2018), suggesting HD-related aberrations during development of the neural tube. While technical limitations of scRNA-seq limit analysis of *Oct4* transcript abundance specifically within the NSC population, our observation of *Oct4* persistence by bulk RNA-seq is corroborated by persistent Oct4 expression found in neuronal differentiations (Conforti et al., 2018). Expression of mHTT impairs Oct4 protein downregulation even in highly expanded repeat lines (60Q, 109Q, 180Q) during differentiation when control cultures transition from pluripotency to neuroectoderm formation. Aberrant maintenance of Oct4 expression in ESC-derived neuronal cultures has also been noted with expanded CAG repeats in other contexts, for example within the hypoxanthine phosphoribosyltransferase (*Hprt*) gene (Lorincz et al., 2004). Temporal dysregulation of other developmental markers has also been observed; juvenile HD iPSCs differentiated toward a striatal fate maintain nestin$^+$ NPCs susceptible to death by brain-derived neurotrophic factor withdrawal, suggesting that mitotically persistent populations of cells are vulnerable to factors mimicking the HD environment (Mattis et al., 2014). These nestin$^+$ NPCs were reduced by targeting the canonical Notch signaling pathway and lowering HTT by antisense oligonucleotide treatment (Mathkar et al., 2019). Additionally, transcriptomic analysis of HD iPSC isogenic lines showed that differences related to neuronal development and dorsal striatum formation occur at the NSC stage (Ring et al., 2015), further implicating the NSC stage in manifestation of developmental aberrations due to mHTT expression. In HD patient iPSC-derived neural cultures, one-third of all gene expression changes were related to pathways involved in neuronal development and maturation (HD iPSC Consortium, 2017).

Several studies have implicated mitotic persistence in altered neurogenesis in HD (Agus et al., 2019; Ooi et al., 2019). ESC-isogenic HD lines differentiated into forebrain neuronal cultures showed altered transcriptional signatures for cell-cycle progression. Other studies implicated cell-cycle re-entry as a mechanism of mitotic dysregulation in HD (Ditsworth et al., 2017; Liu et al., 2015; Pelegrí et al., 2008) and other neurodegenerative diseases (Höglinger et al., 2007; Seward et al., 2013). In contrast, our data indicate a failure to exit the cell cycle as the primary mechanism of persistent mitosis. It is possible that rare cells persist randomly and give rise to a proliferating population during differentiation as opposed to a specific mHTT-mediated effect; however, this is unlikely given that this persistent mitotic population is only observed in the adult-onset lines, not control lines, and is present in all adult-onset lines tested (n = 4). Furthermore, scRNA-seq data showed no clusters having significant differentially expressed levels of *CCND1* between HD and control cells that also showed high levels of mature neuronal marker expression, which would be expected if mature neurons were re-entering the cell cycle.

The work presented offers a mechanism for mitotic persistence, aberrant WNT signaling leading to propagation of mitotic cell populations. This prolonged mitotic state may underlie the transient excess neurogenesis observed in animal models of HD and patient adult striatum (Curtis et al., 2003; Ernst et al., 2014; Tattersfield et al., 2004). Altered WNT signaling is implicated in HD pathogenesis. β-Catenin pathway modulation rescued the toxic effects of mHTT expression and increased the life span in HD *Drosophila*, attenuated neurodegeneration of primary striatal neurons (Godin et al., 2010), and WNT dysregulation may promote aberrant angiogenesis-related signaling observed in HD iPSC-brain microvascular endothelial cells (Lim et al., 2017), suggesting that this pathway may be critical in understanding primary mechanisms affected as a consequence of chronic mHTT expression.

While HTT interacts with the β-catenin destruction complex *in vitro* and *in vivo*, the expanded polyQ region in mHTT prevents binding, leading to toxic β-catenin stabilization and eventual neurodegeneration (Godin et al., 2010). One possibility for the presence of the NSC population only in adult-onset and not in juvenile-range repeat HD neuronal cultures is a threshold activation of the WNT pathway controlled by polyQ length. In neurons, highly expanded polyQ lengths may cause structural changes different from those observed in adult-onset cases that further dysregulate protein-protein interactions and downstream signaling (Caron et al., 2013) such that the highly expanded polyQ region no longer prevents β-catenin from binding the destruction complex and allows for β-catenin degradation, thus preventing transcription of WNT targets such as *CCND1* and *Oct4*. This could allow juvenile lines to follow the same developmental paradigm as control lines without the presence of aberrant NSCs in neuronal populations.

Many neuronal induction protocols exploit inhibition of the WNT pathway due to its role in determining neural crest cell fate (Menendez et al., 2011); two striatal differentiation protocols add the WNT inhibitor DKK1 after initial neural induction (Aubry et al., 2008; Delli Carri et al., 2013). Consistent with the hypothesis that WNT may be differentially activated in the adult-onset versus juvenile-repeat striatal-enriched neuronal cultures, RNA-seq showed that β-catenin destruction complex members were downregulated in adult-onset lines compared with similar levels of both *APC* and *GSK3β* in control and juvenile lines (data not shown). With the addition of CHIR99021, the WNT agonist, in our protocol, the adult-onset lines may no longer be able to compensate for the overactivation of WNT, thereby uncovering a previously undefined mechanism.

We expected to uncover myriad cell-intrinsic differences between control and juvenile HD neuronal cultures and were surprised to find few transcriptional differences. This may be informative for the neurodegenerative disease field in the context of pure populations of iPSC-derived cell types to investigate cell-intrinsic effects. Furthermore, these findings perhaps highlight the phenotypic differences observed between adult- and juvenile-repeat HD, which present quite differently, with manifestation of dyskinesia and global neurodegeneration observed in juvenile cases not present with adult onset (Ruocco et al., 2006). We do not know whether the lack of transcriptional differences between control and juvenile groups is a consequence of (1) juvenile-repeat cell cultures bypassing some point in the differentiation process, (2) cells within the juvenile-repeat lines that remain as NSCs being highly susceptible to cell death, (3) the length of the polyQ repeat expansion acting as flexible domain that modulates the spatial proximity of N17 and polyproline-flanking domains, thereby affecting downstream signaling (Caron et al., 2013), or (4) the need for signals from other cell types for full manifestation of disease. However, regarding point (4), scRNA-seq data from *MAP2*$^{+}$, *NES*/*SOX2*$^{-}$ neurons identifies genes known to be dysregulated in HD neurons, suggesting that there are HD signatures in adult-onset iPSC-derived neurons that overlap with previously published data (HD iPSC Consortium, 2017). The protocol used here reflects very early cell-intrinsic effects. Thus far, we have observed the mitotic population of cells in all adult-onset lines differentiated with this protocol, but only rarely in juvenile-repeat lines and never in control lines.

Overall, our data show that there is a persistent, mitotically active cell population unique to adult-onset repeat

HD cell lines that we can prevent *in vitro* by targeting the WNT pathway with the application of the WNT inhibitor ICG. While ICG is used as a tool to demonstrate the mechanism behind the persistence of NSCs in the context of HD, we speculate that specific components of the WNT signaling pathway inhibited by ICG could be therapeutic targets for HD with the potential to compensate for neurodevelopmental defects.

EXPERIMENTAL PROCEDURES

Products were purchased from Thermo Fisher Scientific (Waltham, MA, USA), unless stated. See Supplemental Information for additional experimental procedures and buffer formulations.

iPSC Differentiation

iPSC lines were generated as described by HD iPSC Consortium (2017). iPSCs were cultured on hESC-qualified Matrigel (Corning) in mTESR1 (STEMCELL Technologies) and passaged with Versene (Gibco). At 60%–70% confluency, medium was changed to start neural differentiation as described by Telezhkin et al. (2016) However, at day 8 cells were replated in activin A-containing medium (see Supplemental Experimental Procedures).

Immunofluorescence

Cells grown on glass coverslips were fixed with 4% paraformaldehyde (PFA; Electron Microscopy Sciences) in PBS for 10 min. Antibody incubations and imaging are described in Supplemental Experimental Procedures.

RNA-Seq

Total RNA was isolated using the Qiagen RNeasy Kit and QIAshredders for cell lysis. One microgram of RNA with RNA integrity number values >9 were used for library preparation using the strand-specific Illumina TruSeq Total RNA protocol. Libraries were sequenced on the HiSeq 2500 platform using 100 cycles to obtain paired-end 100 reads at >50 million reads per sample.

scRNA-Seq

Samples for scRNA-seq were harvested using Dispase (Gibco) for 30 min at 37°C, pipetted off the plate with advanced DMEM/F12 (1:1) with 2% B27, and collected by centrifugation. Cells in 0.1% BSA PBS were filtered through a 70-μm cell strainer and counted. Cells were resuspended at 700 cells/μL in 0.04% BSA in PBS at >80% viability.

ChIP-Seq

Frozen cell pellets (minimum of two replicates per line) were resuspended in lysis buffer and incubated on ice for 20 min. Chromatin was digested and samples processed as described in Supplemental Experimental Procedures. Libraries were prepared using NEBNExt Ultra II DNA Library Prep Kit for Illumina (NEB) and sequenced on an Illumina HiSeq 2000 for single-end 50-bp reads.

ATAC-Seq

Cryostored cell samples were processed in duplicates as previously described (Milani et al., 2016). The ATAC-seq libraries were sequenced on an Illumina HiSeq 2000 for single-end 50-bp reads.

Data Processing

For RNA-seq, fastq files were trimmed using a base quality score threshold of >20 and aligned to the hg19 genome with TopHat 2. Reads passing quality control were used for quantification using HTSeq and analyzed with the R package DESeq2 to identify DEGs. Genes passing an FDR of 10% were used for GO enrichment analysis using GOrilla (Eden et al., 2007, 2009) (http://cbl-gorilla.cs.technion.ac.il/).

For scRNA-seq, fastq files were quality controlled and aligned to the reference transcriptome to obtain a gene count matrix. Before downstream tertiary analysis, quality control of cells was performed by filtering out low-quality cells and low-abundance genes. After quality control and expression matrix formation, normalization was performed using UMI (unique molecular identifiers), and log transformation was used to control variance. Dimension reduction was used to visualize and explore major features of the data using PCA and t-SNE, and differential expression statistical analyses were performed using Seurat and Scanpy. Cell types were assigned based on known cell-type markers.

For ChIP-seq, fastq files were aligned to the hg38 genome assembly using Bowtie2. The ENCODE blacklist regions and PCR duplicates were removed (using SAMtools and Picard). Peak calling was done using MACS2 (–broad flag, q-value < 0.1). Differential analysis of the peaks was performed with Diffbind (Ross-Innes et al., 2012) (http://bioconductor.org/packages/DiffBind/), using EdgeR with FDR <0.05. Differential peaks were annotated to genes within a window of 10 kb from the TSS. GO enrichment analysis was done using Panther (Mi et al., 2012; Thomas et al., 2003) (http://pantherdb.org/webservices/go/overrep.jsp).

For ATAC-seq, fastq files were aligned to hg38 genome assembly using Bowtie2. ENCODE blacklist regions and PCR duplicates were removed (using SAMtools and Picard). Peak calling was done using MACS2 (–nomodel –shift −100 –extsize 200 settings and q-value < 0.05). The consensus peak file for all samples was generated using Diffbind.

Motif Analysis

HOMER (v.4.9.1) was used to identify TF motifs that are enriched in the differential ChIP-seq peaks. ATAC-seq data were used to identify TF-binding locations; thus, for motif analysis we considered consensus ATAC-seq peaks that overlap with the aforementioned differential ChIP-seq peaks. To identify enriched motifs, we used the findMotifs function in HOMER with default parameters; we looked for motif enrichment in the consensus ATAC-seq peaks within ChIP-seq differential peaks compared with a background of all consensus ATAC-seq peaks that are within 10 kb of the TSS of any gene.

Flow Cytometry

Neuronal cultures were harvested at day 37 and fixed in suspension with 4% PFA. Aliquots of cells were made for FMO (Fluorescence Minus One) and unstained controls pooled from all samples

incubated for 2 h at room temperature with primary antibody, washed three times, and incubated with secondary antibody for 30 min. Cells were washed and resuspended in FACS (fluorescence-activated cell sorting) buffer, pipetted through a cell strainer (Falcon), and run on a BD LSRII flow-cytometry machine. Gating was performed using BD FACSDiva software. Further analysis was performed using De Novo FCS Express 6.

Western Blotting

Cells for western blots were scraped and harvested in cold PBS-Mg^{2+}/-Ca^{2+} and flash frozen until processing. Analysis was performed using the LI-COR Odyssey CLx imaging system (see Supplemental Experimental Procedures).

Statistical Analysis

Error bars represent the mean ± SEM where stated. One-tailed t tests were used for comparison of two groups of data. For dataset comparisons of three or more, one-way ANOVA was used; for comparing datasets with two variables among multiple samples, two-way ANOVA was used as stated. Statistical analyses were performed using GraphPad Prism v.8 using $p < 0.05$ as significant. Further information from statistical tests not in figure legends can be found in Tables S3 and S4. For specific assay statistical information, see Supplemental Experimental Procedures.

ACCESSION NUMBERS

All data and code are available from the corresponding authors upon reasonable request. The accession codes are: ChIP-seq, GEO: GSE144493; ATAC-seq, GEO: GSE144518; RNA-seq, GEO: GSE144559; scRNA-seq, GEO: GSE144477.

SUPPLEMENTAL INFORMATION

Supplemental Information can be found online at https://doi.org/10.1016/j.stemcr.2020.01.015.

AUTHOR CONTRIBUTIONS

L.M.T., E.F., C.S.-G., and S.J.H. conceived and designed the experiments. C.S.-G., S.J.H., M.A., J.T.S., K.Q.W., L.K., and I.O. performed the experiments and carried out data analysis. S.J., C.S.-G., N.D.A., and P.J.K. developed the differentiation paradigm. R.G.L., J.W., B.T.W., M.P.G., and R.M. performed omics data analysis. S.J.H., C.S.-.G., M.A., R.G.L., E.F., and L.M.T. wrote the manuscript. L.M.T. and E.F. supervised the project and acquired funding.

ACKNOWLEDGMENTS

We thank the HD patients and their families for their essential contributions to this research and Dr. David Housman for helpful discussions of the data. Primary support for this work was from NIH NS089076 (L.M.T., E.F.) and the CHDI Foundation (P.J.K., N.D.A.). Additional support was provided by NIH (U54 NS091046 NeuroLINCS center, L.M.T., E.F.; NIH NS078370, L.M.T., E.F.), California Institute for Regenerative Medicine (CIRM) (C.S.-G.), the Hereditary Disease Foundation (C.S.-G.), the UCI Institute for Clinical and Translational Science (L.M.T.), HDSA Berman/Topper Career Development Fellowship (S.J.H.), HD CARE (L.M.T.), NIH T32 grant TG32 AG00096 (S.J.H.), and the UK Medical Research Council (P.J.K. and N.D.A.). This work was made possible, in part, through access to the Genomic High Throughput Facility Shared Resource of the Cancer Center Support grant (CA-62203) at the University of California, Irvine. Support also included computing resources from National Science Foundation grant DB1-0821391 and sequencing support from National Institutes of Health grant P30-ES002109. The authors declare no competing interests.

Received: August 19, 2019
Revised: January 30, 2020
Accepted: January 31, 2020
Published: February 27, 2020

REFERENCES

Agus, F., Crespo, D., Myers, R.H., and Labadorf, A. (2019). The caudate nucleus undergoes dramatic and unique transcriptional changes in human prodromal Huntington's disease brain. BMC Med. Genomics *12*, 137.

Arber, C., Precious, S.V., Cambray, S., Risner-Janiczek, J.R., Kelly, C., Noakes, Z., Fjodorova, M., Heuer, A., Ungless, M.A., Rodriguez, T.A., et al. (2015). Activin A directs striatal projection neuron differentiation of human pluripotent stem cells. Development *142*, 1375–1386.

Arlotta, P., Molyneaux, B.J., Jabaudon, D., Yoshida, Y., and Macklis, J.D. (2008). Ctip2 controls the differentiation of medium spiny neurons striatum. J. Neurosci. *28*, 622–632.

Aubry, L., Bugi, A., Lefort, N., Rousseau, F., Peschanski, M., and Perrier, A.L. (2008). Striatal progenitors derived from human ES cells mature into DARPP32 neurons in vitro and in quinolinic acid-lesioned rats. Proc. Natl. Acad. Sci. U S A *105*, 16707–16712.

Beattie, G.M., Lopez, A.D., Bucay, N., Hinton, A., Firpo, M.T., King, C.C., and Hayek, A. (2005). Activin A maintains pluripotency of human embryonic stem cells in the absence of feeder layers. Stem Cells *23*, 489–495.

Bowles, K.R., Stone, T., Holmans, P., Allen, N.D., Dunnett, S.B., and Jones, L. (2017). SMAD transcription factors are altered in cell models of HD and regulate HTT expression. Cell. Signal. *31*, 1–14.

Buckley, N.J., Johnson, R., Zuccato, C., Bithell, A., and Cattaneo, E. (2010). The role of REST in transcriptional and epigenetic dysregulation in Huntington's disease. Neurobiol. Dis. *39*, 28–39.

Caron, N.S., Desmond, C.R., Xia, J., and Truant, R. (2013). Polyglutamine domain flexibility mediates the proximity between flanking sequences in huntingtin. Proc. Natl. Acad. Sci. U S A *110*, 14610–14615.

Carri, A.D., Onorati, M., Castiglioni, V., Faedo, A., Camnasio, S., Toselli, M., Biella, G., and Cattaneo, E. (2013). Human pluripotent stem cell differentiation into authentic striatal projection neurons. Stem Cell Rev. Rep. *9*, 461–474.

Conforti, P., Besusso, D., Bocchi, V.D., Faedo, A., Cesana, E., Rossetti, G., Ranzani, V., Svendsen, C.N., Thompson, L.M., Toselli, M., et al. (2018). Faulty neuronal determination and cell polarization are reverted by modulating HD early phenotypes. Proc. Natl. Acad. Sci. U S A *115*, E762–E771.

Cronin, T., Rosser, A., and Massey, T. (2019). Clinical presentation and features of Juvenile-onset Huntington's disease: a systematic review. J. Huntingtons Dis. *8*, 171–179.

Curtis, M.A., Penney, E.B., Pearson, A.G., Van Roon-mom, W.M.C., Butterworth, N.J., Dragunow, M., Connor, B., and Faull, R.L.M. (2003). Increased cell proliferation and neurogenesis in the adult human Huntington's disease brain. Proc. Natl. Acad. Sci. U S A *100*, 9023–9027.

Curtis, M.A., Penney, E.B., Pearson, J., Dragunow, M., Connor, B., and Faull, R.L.M. (2005). The distribution of progenitor cells in the subependymal layer of the lateral ventricle in the normal and Huntington's disease human brain. Neuroscience *132*, 777–788.

Delli Carri, A., Onorati, M., Lelos, M.J., Castiglioni, V., Faedo, A., Menon, R., Camnasio, S., Vuono, R., Spaiardi, P., Talpo, F., et al. (2013). Developmentally coordinated extrinsic signals drive human pluripotent stem cell differentiation toward authentic DARPP-32+ medium-sized spiny neurons. Dev. Stem Cells *140*, 301–312.

Ditsworth, D., Maldonado, M., McAlonis-Downes, M., Sun, S., Seelman, A., Drenner, K., Arnold, E., Ling, S.-C., Pizzo, D., Ravits, J., et al. (2017). Mutant TDP-43 within motor neurons drives disease onset but not progression in amyotrophic lateral sclerosis. Acta Neuropathol. *133*, 907–922.

Eden, E., Lipson, D., Yogev, S., and Yakhini, Z. (2007). Discovering motifs in ranked lists of DNA sequences. PLoS Comput. Biol. *3*, e39.

Eden, E., Navon, R., Steinfeld, I., Lipson, D., and Yakhini, Z. (2009). GOrilla: a tool for discovery and visualization of enriched GO terms in ranked gene lists. BMC Bioinformatics *10*, 48.

Emami, K.H., Nguyen, C., Ma, H., Kim, D.H., Jeong, K.W., Eguchi, M., Moon, R.T., Teo, J.-L., Oh, S.W., Kim, H.Y., et al. (2004). A small molecule inhibitor of β-catenin/cyclic AMP response element-binding protein transcription. Proc. Natl. Acad. Sci. U S A *101*, 12682–12687.

Ernst, A., Alkass, K., Bernard, S., Salehpour, M., Perl, S., Tisdale, J., Possnert, G., Druid, H., and Frisen, J. (2014). Neurogenesis in the striatum of the adult human brain. Cell *156*, 1072–1083.

Godin, J.D., Poizat, G., Hickey, M.A., Maschat, F., and Humbert, S. (2010). Mutant huntingtin-impaired degradation of β-catenin causes neurotoxicity in Huntington's disease. EMBO J. *29*, 2433–2445.

Guo, X., Disatnik, M.-H., Monbureau, M., Shamloo, M., Mochly-Rosen, D., and Qi, X. (2013). Inhibition of mitochondrial fragmentation diminishes Huntington's disease-associated neurodegeneration. J. Clin. Invest. *123*, 5371–5388.

HD iPSC Consortium (2017). Developmental alterations in Huntington's disease neural cells and pharmacological rescue in cells and mice. Nat. Neurosci. *20*, 648–660.

Höglinger, G.U., Breunig, J.J., Depboylu, C., Rouaux, C., Michel, P.P., Alvarez-Fischer, D., Boutillier, A.-L., DeGregori, J., Oertel, W.H., Rakic, P., et al. (2007). The pRb/E2F cell-cycle pathway mediates cell death in Parkinson's disease. Proc. Natl. Acad. Sci. U S A *104*, 3585–3590.

Hughes, T.A., and Brady, H.J.M. (2005). Cross-talk between pRb/E2F and Wnt/β-catenin pathways: E2F1 induces axin2 leading to repression of Wnt signalling and to increased cell death. Exp. Cell Res. *303*, 32–46.

Huntington's Disease Collaborative Research Group (1993). A novel gene containing a trinucleotide repeat that is expanded and unstable on Huntington's disease chromosomes. Cell *72*, 971–983.

Lazic, S.E., Grote, H., Armstrong, R.J.E., Blakemore, C., Hannan, A.J., van Dellen, A., and Barker, R.A. (2004). Decreased hippocampal cell proliferation in R6/1 Huntington's mice. Neuroreport *15*, 811–813.

Lim, R.G., Quan, C., Reyes-Ortiz, A.M., Housman, D.E., Agalliu, D., Thompson, L.M., Lim, R.G., Quan, C., Reyes-ortiz, A.M., Lutz, S.E., et al. (2017). Huntington's disease iPSC-derived brain microvascular endothelial cells reveal WNT- article Huntington's disease iPSC-derived brain microvascular endothelial cells reveal WNT-mediated angiogenic and blood-brain barrier deficits. Cell Rep. *19*, 1365–1377.

Liu, K.Y., Shyu, Y.C., Barbaro, B.A., Lin, Y.T., Chern, Y., Thompson, L.M., Shen, C.K.J., and Marsh, J.L. (2015). Disruption of the nuclear membrane by perinuclear inclusions of mutant huntingtin causes cell-cycle re-entry and striatal cell death in mouse and cell models of Huntington's disease. Hum. Mol. Genet. *24*, 1602–1616.

Lorincz, M.T., Detloff, P.J., Albin, R.L., and O'Shea, K.S. (2004). Embryonic stem cells expressing expanded CAG repeats undergo aberrant neuronal differentiation and have persistent Oct-4 and REST/NRSF expression. Mol. Cell. Neurosci. *26*, 135–143.

Lo Sardo, V., Zuccato, C., Gaudenzi, G., Vitali, B., Ramos, C., Tartari, M., Myre, M.A., Walker, J.A., Pistocchi, A., Conti, L., et al. (2012). An evolutionary recent neuroepithelial cell adhesion function of huntingtin implicates ADAM10-Ncadherin. Nat. Neurosci. *15*, 713–721.

Mathkar, P.P., Suresh, D., Dunn, J., Tom, C.M., and Mattis, V.B. (2019). Characterization of neurodevelopmental abnormalities in iPSC-derived striatal cultures from patients with Huntington's disease. J. Huntingtons Dis. *8*, 257–269.

Mattis, V.B., Tom, C., Akimov, S., Saeedian, J., Østergaard, M.E., Southwell, A.L., Doty, C.N., Ornelas, L., Sahabian, A., Lenaeus, L., et al. (2014). HD iPSC-derived neural progenitors accumulate in culture and are susceptible to BDNF withdrawal due to glutamate toxicity. Hum. Mol. Genet. *24*, 3257–3271.

Menendez, L., Yatskievych, T.A., Antin, P.B., and Dalton, S. (2011). Wnt signaling and a Smad pathway blockade direct the differentiation of human pluripotent stem cells to multipotent neural crest cells. Proc. Natl. Acad. Sci. U S A *108*, 19240–19245.

Mi, H., Muruganujan, A., and Thomas, P.D. (2012). PANTHER in 2013: modeling the evolution of gene function, and other gene attributes, in the context of phylogenetic trees. Nucleic Acids Res. *41*, D377–D386.

Milani, P., Escalante-Chong, R., Shelley, B.C., Patel-Murray, N.L., Xin, X., Adam, M., Mandefro, B., Sareen, D., Svendsen, C.N., and Fraenkel, E. (2016). Cell freezing protocol suitable for ATAC-Seq on motor neurons derived from human induced pluripotent stem cells. Sci. Rep. *6*, 25474.

Molero, A.E., Gokhan, S., Gonzalez, S., Feig, J.L., Alexandre, L.C., and Mehler, M.F. (2009). Impairment of developmental stem cell-mediated striatal neurogenesis and pluripotency genes in a knock-in model of Huntington's disease. Proc. Natl. Acad. Sci. U S A *106*, 21900–21905.

Ooi, J., Langley, S.R., Xu, X., Utami, K.H., Sim, B., Huang, Y., Harmston, N.P., Tay, Y.L., Ziaei, A., Zeng, R., et al. (2019). Unbiased profiling of isogenic huntington disease hPSC-derived CNS and peripheral cells reveals strong cell-type specificity of CAG length effects. Cell Rep. *26*, 2494–2508.e7.

Pelegrí, C., Duran-Vilaregut, J., del Valle, J., Crespo-Biel, N., Ferrer, I., Pallàs, M., Camins, A., and Vilaplana, J. (2008). Cell cycle activation in striatal neurons from Huntington's disease patients and rats treated with 3-nitropropionic acid. Int. J. Dev. Neurosci. *26*, 665–671.

Phillips, W., Morton, A.J., and Barker, R.A. (2005). Abnormalities of neurogenesis in the R6/2 mouse model of Huntington's disease are attributable to the in vivo microenvironment. J. Neurosci. *25*, 11564–11576.

Poon, A., Zhang, Y., Chandrasekaran, A., Phanthong, P., Schmid, B., Nielsen, T.T., and Freude, K.K. (2017). Modeling neurodegenerative diseases with patient-derived induced pluripotent cells: possibilities and challenges. Nat. Biotechnol. *39*, 190–198.

Ring, K.L., An, M.C., Zhang, N., O'Brien, R.N., Ramos, E.M., Gao, F., Atwood, R., Bailus, B.J., Melov, S., Mooney, S.D., et al. (2015). Genomic analysis reveals disruption of striatal neuronal development and therapeutic targets in human Huntington's disease neural stem cells. Stem Cell Reports *5*, 1023–1038.

Ross-Innes, C.S., Stark, R., Teschendorff, A.E., Holmes, K.A., Ali, H.R., Dunning, M.J., Brown, G.D., Gojis, O., Ellis, I.O., Green, A.R., et al. (2012). Differential oestrogen receptor binding is associated with clinical outcome in breast cancer. Nature *481*, 389–393.

Ruocco, H.H., Lopes-Cendes, I., Laurito, T.L., Li, L.M., and Cendes, F. (2006). Clinical presentation of juvenile Huntington disease. Arq. Neuropsiquiatr. *64*, 5–9.

Ruzo, A., Croft, G.F., Metzger, J.J., Galgoczi, S., Gerber, L.J., Pellegrini, C., Wang, H., Fenner, M., Tse, S., Marks, A., et al. (2018). Chromosomal instability during neurogenesis in Huntington's disease. Development *145*. https://doi.org/10.1242/dev.156844.

Seward, M.E., Swanson, E., Norambuena, A., Reimann, A., Cochran, J.N., Li, R., Roberson, E.D., and Bloom, G.S. (2013). Amyloid-β signals through tau to drive ectopic neuronal cell cycle re-entry in Alzheimer's disease. J. Cell Sci. *126*, 1278–1286.

Shi, Y., Shu, B., Yang, R., Xu, Y., Xing, B., Liu, J., Chen, L., Qi, S., Liu, X., Wang, P., et al. (2015). Wnt and Notch signaling pathway involved in wound healing by targeting c-Myc and Hes1 separately. Stem Cell Res. Ther. *6*, 120.

Tabrizi, S.J., Ghosh, R., and Leavitt, B.R. (2019). Huntingtin lowering strategies for disease modification in Huntington's disease. Neuron *101*, 801–819.

Tattersfield, A.S., Croon, R.J., Liu, Y.W., Kells, A.P., Faull, R.L.M., and Connor, B. (2004). Neurogenesis in the striatum of the quinolinic acid lesion model of Huntington's disease. Neuroscience *127*, 319–332.

Telezhkin, V., Schnell, C., Yarova, P., Yung, S., Cope, E., Hughes, A., Thompson, B.A., Sanders, P., Geater, C., Hancock, J.M., et al. (2016). Forced cell cycle exit and modulation of GABAA, CREB, and GSK3β signaling promote functional maturation of induced pluripotent stem cell-derived neurons. Am. J. Physiol. Cell Physiol. *310*, C520–C541.

The HD iPSC Consortium (2012). Induced pluripotent stem cells from patients with Huntington's disease show CAG-repeat-expansion-associated phenotypes. Cell Stem Cell *11*, 264–278.

Thomas, P.D., Campbell, M.J., Kejariwal, A., Mi, H., Karlak, B., Daverman, R., Diemer, K., Muruganujan, A., and Narechania, A. (2003). PANTHER: a library of protein families and subfamilies indexed by function. Genome Res. *13*, 2129–2141.

Valor, L.M. (2015). Transcription, epigenetics and ameliorative strategies in Huntington's disease: a genome-wide perspective. Mol. Neurobiol. *51*, 406–423.

Wiatr, K., Szlachcic, W.J., Trzeciak, M., Figlerowicz, M., and Figiel, M. (2018). Huntington disease as a neurodevelopmental disorder and early signs of the disease in stem cells. Mol. Neurobiol. *55*, 3351–3371.

Yeo, H.C., Beh, T.T., Quek, J.J.L., Koh, G., Chan, K.K.K., and Lee, D.-Y. (2011). Integrated transcriptome and binding sites analysis implicates E2F in the regulation of self-renewal in human pluripotent stem cells. PLoS One *6*, e27231.